

RESEARCH

Open Access



Immunological enhancement of micro-nanoparticle formulated with risedronate and zinc as vaccine adjuvant in aged mice

Yue Liu^{1†}, Man Yang^{1†}, Meifeng Nie¹, Shuyu Wu¹, Rong Su¹, Dekui Qiu¹, Shouneng Lu¹, Hualong Xiong¹, Jinlei Zhang¹, Shengxiang Ge¹, Quan Yuan¹, Qinjian Zhao^{2*}, Tianying Zhang^{1*}, Yingbin Wang^{1*} and Ningshao Xia¹

Abstract

Background Elderly individuals face heightened susceptibility to infectious diseases and diminished vaccine responses. Vaccine adjuvants offer a solution. Despite aluminum adjuvant's long history, its limitations in inducing strong cellular immunity and protecting immunocompromised individuals restrict its application. Building upon our previous development of zinc salt particle-based risedronate (Zn-RS), we systematically investigated the immunoenhancing effects of Zn-RS in aged mice and thoroughly explored the underlying mechanisms responsible for these observations in this study.

Results Compared to formulations using aluminum adjuvant, Zn-RS combined with either varicella-zoster virus glycoprotein E (gE) or SARS-CoV-2 monovalent STFK protein (STFK) elicited significantly higher IgG and neutralization titers, as well as superior long-term humoral immunity. Moreover, Zn-RS induced greater quantities of dendritic cells (DCs), antigen-presenting cells (APCs), follicular helper T (T_{FH}) cells, Th1/Th2/Th9/Th17 type immune cells, germinal center B cells (GCBs) and plasma cells.

Conclusions These findings support Zn-RS as a promising adjuvant candidate for elderly populations, warranting further exploration of its mechanisms and potential applications.

Keywords Risedronate, Vaccine adjuvant, Aged mice, Immune enhancement, Mechanism

[†]Yue Liu and Man Yang contributed equally to this work.

*Correspondence:

Qinjian Zhao
zhaoqinjian@cqmu.edu.cn
Tianying Zhang
zhangtianying@xmu.edu.cn
Yingbin Wang
ybwang@xmu.edu.cn

¹ State Key Laboratory of Vaccines for Infectious Diseases, Xiang An Biomedicine Laboratory, School of Public Health & School of Life Sciences, Xiamen University, Xiamen, Fujian 361102, China

² College of Pharmacy, Chongqing Medical University, Chongqing 400016, China



Introduction

Aging is an inevitable, multifaceted process that occurs universally. Although vaccines designed to target multiple pathogens have saved millions of lives worldwide, their efficacy in elderly individuals is frequently diminished by immunosenescence, characterized by the age-related deterioration of immune responses [1–3]. With the increasing proportion of elderly individuals worldwide and the elevated risk of infectious disease pandemics, research and development of vaccines and adjuvant systems that provide effective immune protection for older adults are crucial for promoting healthy aging worldwide and preventing severe diseases [4].

Adjuvants enhance vaccine effectiveness by employing multiple mechanisms, including stimulation of pro-inflammatory cytokine production, recruitment and activation of innate immune cells, engagement of pattern recognition receptors (PRRs) on immune cells, and potentiation of antigen presentation processes. Previous research has revealed that the directed transport of subunit vaccines requires the ability to navigate a complex in vivo cascade process involving six critical steps: initiating targeted delivery to lymph nodes, followed by specific targeting of dendritic cell (DC) subsets, modulation of B cells, antigen-internalization and cross-presentation, and finally, regulation of antigen-presenting cells (APCs) to elicit T-cell activation. However, in elderly individuals, the quantity of naïve T cells drops relative to that observed in younger individuals, thereby impairing the immune response to previously unencountered antigens. Concurrently, changes in DC function encompass impaired migratory capacity and reduced synthesis of specific cytokines, both of which are indispensable for eliciting T-cell-mediated protective immunological responses [5, 6]. To counteract age-associated declines in vaccine efficacy, enhancing the proliferation of DCs could constitute a promising and efficacious strategy.

Bisphosphonates (BPs) are synthetic drugs that are utilized for therapeutic applications in bone diseases and feature a highly stable phosphorus-backbone-phosphorus structure, which provides increased affinity to the hydroxyapatite in bones [7, 8]. BPs are classified into two main categories: those with nitrogen content (N-BPs) and those without nitrogen content (non-N-BPs), of which N-BPs induce stronger immune responses. Studies have indicated that the application of pamidronic acid results in a higher proportion of γ/δ T cells [9]. Furthermore, zoledronic acid can activate and expand natural killer (NK) cells, DCs, and γ/δ T cells, which exhibit cytotoxic effects on various solid tumor cell lines [10, 11]. Zinc, ranking second only to iron among trace elements in the human body, plays a vital role in exchanging information between cells, mediating processes of

cell division and differentiation, and immune modulation [12]. Decreased serum zinc levels are correlated with impaired neutrophil chemotaxis, reduced macrophage phagocytosis, increased apoptosis, and a diminished capacity of NK cells to secrete cytokines such as tumor necrosis factor- α (TNF- α) and interferon- γ (IFN- γ) [13, 14]. Zinc is indispensable for orchestrating the proliferation, differentiation, and polarization of T helper (Th) cells. Additionally, reduced serum zinc levels are correlated with increased B lymphocyte apoptosis, compromised B-cell maturation and impaired receptor signaling [15, 16]. According to World Health Organization (WHO) statistics, the zinc deficiency rate of the population worldwide is approximately 17% to 20%, and elderly individuals are more likely to develop zinc deficiency [17]. Zinc supplementation can reduce systemic inflammation and enhance the efficacy of vaccinations, while investigations into the prophylactic efficacy of a hybrid particulate adjuvant (aluminum-zinc) against influenza have demonstrated that zinc significantly contributes to immune responses [18, 19]. BPs, which contain two phosphate groups in combination with zinc salts, show potential as vaccine adjuvants for elderly individuals. Furthermore, it has been reported that a zinc-aluminum hybrid adjuvant modified with N-BPs shows promise as a potential adjuvant in vaccines designed to protect against SARS-CoV-2 infection [20].

Previous studies have shown that the Zinc-Risedronate (Zn-RS) adjuvant has an obvious antibody-enhancing effect on young mice [11]. In this study, we combined Zn-RS adjuvant with wild-type spike monomeric protein (STFK) [21] and varicella-zoster virus glycoprotein E (gE) [22] in aged mice and reported that the Zn-RS adjuvant enhanced the antibody and T-cell response. Mechanistic studies revealed that the Zn-RS adjuvant could enhance the proliferation of DCs, APCs, germinal center B (GCB) cells, plasma cells, and follicular helper T (T_{FH}) cells and promote the secretion of Th1/Th2/Th9/Th17 cytokines. Moreover, abnormal toxicity experiments in KM mice also showed good safety. In summary, this study serves as a valuable foundation for optimizing adjuvant formulations in geriatric vaccinology.

Results

Characterization of the physicochemical properties and abnormal toxicity evaluation of adjuvants

The appearance, particle morphology, and settling properties of emulsions of suspensions serve as key indicators for evaluating their stability. Compared with aluminum salt adjuvant (Al-001), the Zn-RS adjuvant appeared milky white at 0 h. After 24 h, the precipitate of the Zn-RS adjuvant was more solid than that of the Al-001 adjuvant. Under an electron microscope, both the Al-001

and Zn-RS adjuvants exhibited seaweed-like clusters with visible core particles (Fig. 1A). Aside from stability, the physicochemical properties of the adjuvant can be evaluated through its pH, particle size, and point of zero charge (PZC). Zn-RS had a similar pH to that of Al-001. However, the diameter of Zn-RS is smaller than that of Al-001 (Table 1), which may indicate superior adjuvant effects [23]. The two adjuvants demonstrated negative potentials when measured at a neutral pH (Fig. 1B). For the Al-001 and Zn-RS adjuvants, almost complete mineralization of the metal ions and risedronate was achieved (Fig. 1C). Zn-RS exhibited an approximately 90% adsorption rate for STFK, which was lower than that of Al-001 (Fig. 1D).

After administering a 0.5 mL intraperitoneal injection of the adjuvant to the KM mice, all the KM mice in the Zn-RS adjuvant group and the Al-001 adjuvant group (control group) survived over a 7-day observation period, and all the KM mice gained body weight compared with the initial measurements at the conclusion of the observation period (Fig. 1E). These findings indicate that the safety profile of the Zn-RS adjuvant conforms to the criteria set by the pharmacopoeia.

Zn-RS formulated with STFK induced a robust Th1-biased immune response and excellent neutralizing titers in young and elderly mice

We then explored the enhanced immunogenicity of the Zn-RS-adjuvanted STFK vaccine in C57BL/6 mice of two age groups: 1. young (6 weeks old) group; 2. aged (15 months old) group. C57BL/6 mice ($n = 6/\text{group}$) received bilateral intramuscular immunizations with STFK-formulated vaccine (1 $\mu\text{g}/\text{dose}$), with booster administration at 3-week intervals. Humoral immune responses were assessed 14 days after the first shot. Compared with the Al-001-containing STFK formulation, the Zn-RS-containing STFK formulation enhanced the serum antibody titer directed against STFK and the RBD in mice from the two age groups (Fig. 2A, B; I–J). Moreover, sera from animals immunized with the Zn-RS adjuvant formulation exhibited higher titers of anti-STFK IgG1, IgG2a and IgG2b (Fig. 2C–E; K–M), as well as higher IgG2a/IgG1 (Fig. 2F, N) and IgG2b/IgG1 titer ratios (Fig. 2G, O) compared with those of the Al-001 adjuvant formulation.

In conclusion, these findings demonstrated that Zn-RS induced more balanced Th1/Th2 immune responses.

Potent neutralizing antibodies serve as key serological correlates for evaluating vaccine efficacy against emerging SARS-CoV-2 variants. However, novel SARS-CoV-2 strains, such as BA.4/5, demonstrate decreased susceptibility to antibody-dependent neutralization in serum collected from convalescent or immunized individuals [24, 25]. To evaluate the potential of Zn-RS to enhance broad-spectrum neutralizing responses, we measured levels of antibody titers in serum collected from mice administered the vaccine formulated in conjunction with STFK antigens. Although we observed a decline in antibody-mediated neutralization efficacy of BA.4/5 strain compared with those against the wild-type (WT) strain in our mouse model (after two doses of the STFK-Zn-RS vaccine), the Zn-RS-adjuvanted group exhibited significantly greater neutralizing antibody titers than the control group did (Fig. 2H, P). Overall, in combination with the STFK antigen, the Zn-RS adjuvant elicits superior neutralizing capacity against prototype and BA.4/5 strains compare to the Al-001 adjuvant. Furthermore, in the present study, serum antibody titers against STFK and RBD were continuously monitored in both age groups (6 weeks old and 15 months old) of C57BL/6 mice, which were administered Zn-RS and Al-001 immunization formulations over a period of 10 weeks following the initial immunization. In the two age groups, the Zn-RS formulation induced higher titers of anti-STFK- and anti-RBD-binding antibodies than did the Al-001 formulation, which persisted until the 10th week. This effect was more pronounced in aged mice (Fig. 2Q, R).

Zn-RS-adjuvanted gE vaccine enhanced immune responses in young and aged mice

To evaluate systemically the capacity of Zn-RS and Al-001 in inducing humoral versus cellular immunological outcomes, we immunized two age groups (6 weeks old and 15 months old) of C57BL/6 mice with the Zn-RS- or Al-001-adjuvanted gE vaccine. To evaluate the impact of vaccination on the enhancement of antibody titers, we assessed the binding titers two weeks following the initial immunization and one week after the subsequent immunization. As a result, in these two tests, the mice that received gE-Zn-RS presented higher antibody titers than

(See figure on next page.)

Fig. 1 Physicochemical property standards and abnormal toxicity tests of the Zn-RS and Al-001 adjuvants. **A** Macroscopic appearance and representative IEM images of Al-001 and Zn-RS. **B** Zeta potential of adjuvants at pH 7.0. **C** Measurement of metal element contents in adjuvants and their supernatants. The formula used for calculation was as described previously: $[1 - (\text{supernatant metal content}/\text{total metal content})] * 100\%$. Measurements for each metal element were performed in triplicate. **D** The concentration of STFK before combination with adjuvants was 200 $\mu\text{g}/\text{mL}$. **E** Weight changes and survival timeline of KM mice injected intraperitoneally with 0.5 mL of Al-001 or Zn-RS over a 7-day observation period

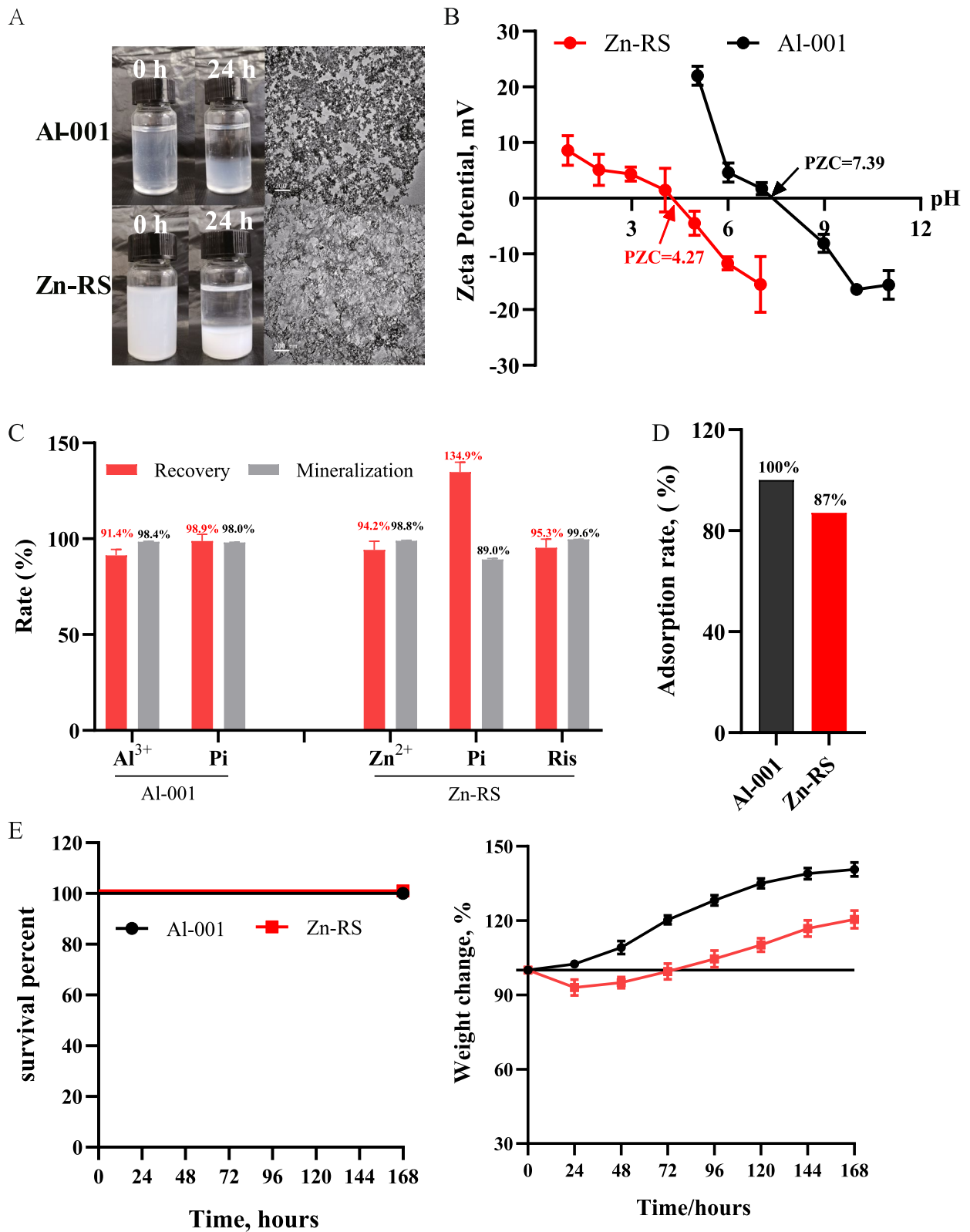


Fig. 1 (See legend on previous page.)

Table 1 pH and particle size of Al-001 and Zn-RS; each measurement was repeated three times

	pH				Diameter, μm			
	1 st	2nd	3rd	AVE + SD	1 st	2nd	3rd	AVE + SD
Al-001	6.30	6.34	6.33	6.32 \pm 0.02	14.84	19.45	15.90	16.73 \pm 1.89
Zn-RS	6.38	6.39	6.40	6.39 \pm 0.01	2.64	2.63	2.54	2.60 \pm 0.04

did those that received gE-Al-001 (Fig. 3A, B). Similarly, data obtained from the serum samples of the two age groups mentioned above demonstrated that the Zn-RS group induced higher binding titers within the 0–5-week period (Fig. 3C, D). In aged mice, the Zn-RS group presented significantly greater neutralizing antibody titers ($P < 0.01$) compared to the Al-001 group (Fig. 3E). In the analysis of gE-specific T-cell responses by IFN- γ ELISpot, peptide stimulation induced 64-fold higher spot-forming unit counts in splenocytes isolated from gE-Zn-RS-immunized young C57BL/6 mice relative to the gE-Al-001 immunization group. Additionally, there was a 3.8-fold increase in the number of lymph node cells. Similarly, in aged mice, gE-Zn-RS was observed to induce an increased secretion of IFN- γ in both the spleen and lymph nodes compared with gE-Al-001 (Fig. 3F). To conduct quantitative immunophenotyping analysis of draining lymph nodes (dLNs), seven days after the second shot, the number of cells that produce IFN- γ or interleukin (IL)-4 within dLNs was measured via flow cytometry. Compared with the Al-001 group, the Zn-RS group demonstrated a higher absolute number of CD4⁺ and CD8⁺ cells that secreted IFN- γ or IL-4 in the two age groups (Fig. 3G–J).

Enhanced antigen presentation capacity was elicited in the Zn-RS-adjuvant group

APCs and LNs are both essential for integrating and regulating natural and adaptive immune responses. Specifically, APCs are responsible for delivering antigens to T cells, and LNs serve as critical sites for integrating immune responses. Overall, they are essential for coordinating adaptive immune responses and enhancing immune responses to vaccines [26, 27]. Activation of innate immune mechanisms triggers an immediate immunological response in LNs characterized by lymphocyte accumulation and upregulated expression of proinflammatory mediators [28, 29]. To further elucidate the functional mechanism of the Zn-RS formulation, we harvested inguinal lymph nodes 7 days post-injection of either the Zn-RS or the Al-001 adjuvant formulation. MF59, a clinically licensed squalene-stabilized oil-in-water emulsion adjuvant, not only enhances Th1 (IFN- γ ⁺)/Th2 (IL-4⁺) T-cell responses but also promotes

germinal center (GC) development [30, 31] and was used as a benchmark adjuvant in this study. When immunized with different formulations, the Zn-RS formulation induced greater proliferation of macrophages, mononuclear cells, neutrophils, DCs and B cells in C57BL/6 mice (6 weeks of age and 15 months of age). Furthermore, the trend was essentially the same in the lymph nodes and spleens (Fig. 4A–C). The results of the binding antibody assay revealed that, compared with the Al-001 group, the Zn-RS group had a greater binding antibody titer. This effect may be attributed to the enhanced proliferation of APCs in the lymph nodes and spleens during the early stages of immunization. These results indicate that comparable pathways may be activated by the Zn-RS adjuvant in mice of different age groups (6 weeks old and 15 months old).

The Zn-RS adjuvant promoted the proliferation of GCB and memory B/T cells

Germinal center responses are essential for inducing robust and sustained B-cell responses, with T_{FH} cells serving as core regulators of these processes [32]. Class-switched, affinity-matured antibodies generated from plasma cells, together with sustained memory B cells, constitute the cornerstone of effective and enduring humoral immunity against infectious agents [33]. Long-lived plasma cell and memory B-cell formation critically relies on the signals provided by T_{FH} cells within GCs [34]. T_{FH} cells are distinctly identified within the CD4⁺ T-cell population by their surface-expressed C-X-C chemokine receptor 5 (CXCR5) and programmed cell death protein 1 (PD-1) [35]. To gain deeper insights into the impact of vaccine adjuvants and age on GC responses and memory B/T responses, we immunized C57BL/6 mice (6 weeks old and 15 months old) with STFK1628x [21] vaccines formulated with Al-001 or Zn-RS. Two weeks after the initial immunization, we measured the number of GC_B, T_{FH}, and plasma cells from the spleen and lymph node tissues of the mice (Fig. 5A). Compared with the Al-001 group, the Zn-RS group presented significantly greater numbers of plasma cells (Fig. 5A), T_{FH} cells (Fig. 5A), and GC_Bs (Fig. 5A). This enhancement was consistent with the swift antibody-mediated immune

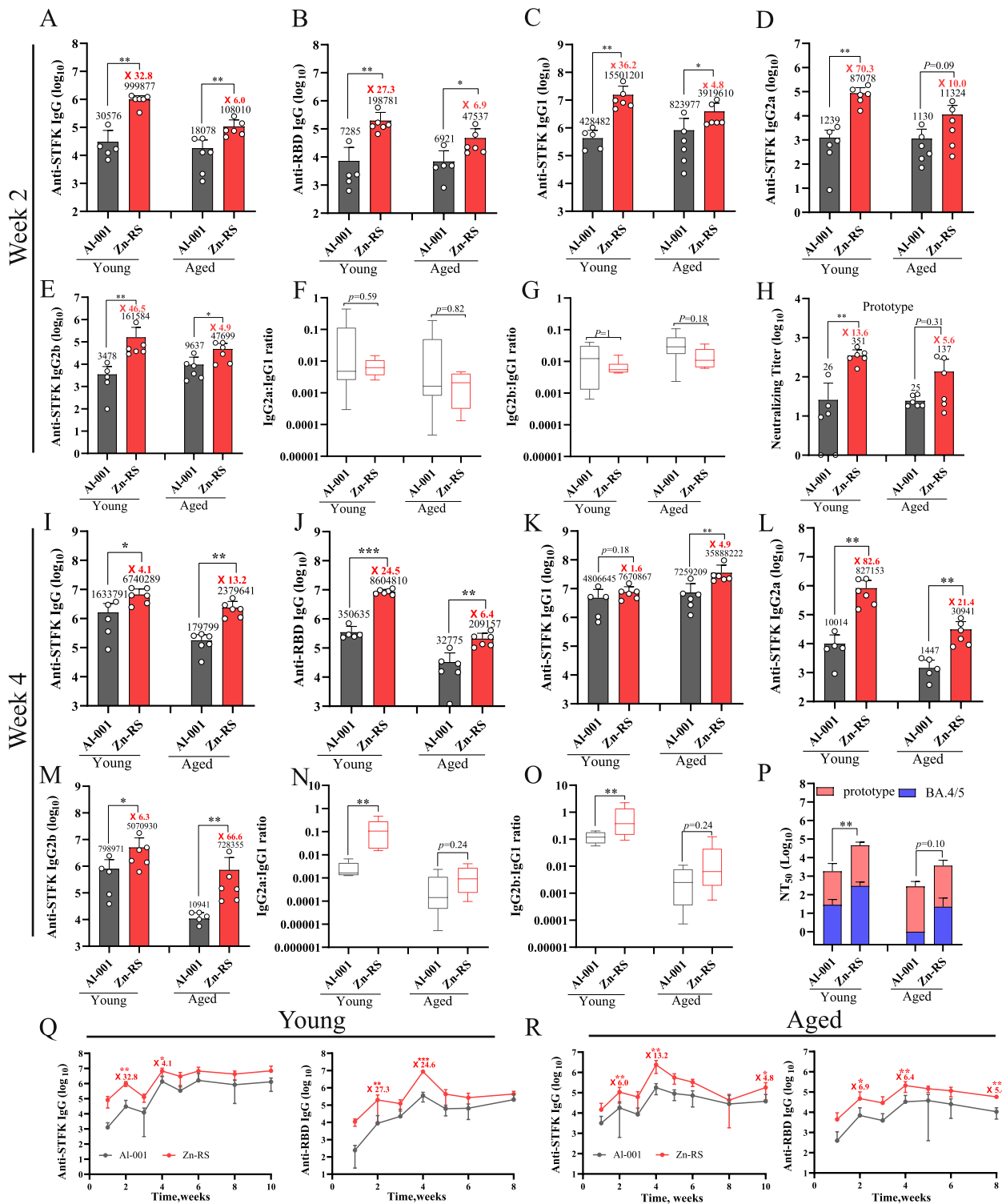


Fig. 2 Antibody responses were induced by STFK formulated with Zn-RS in young and aged mice. Six-week-old and fifteen-month-old C57BL/6 mice were injected intramuscularly on days 0 and 21 with 1 μg of the STFK protein with AI-001 or Zn-RS. Retro-orbital blood was collected on day 14 (**A**–**H**) and day 28 (**I**–**P**). **A** and **I** Binding titers against STFK, **B** and **J** anti-RBD IgG, **C** and **K** anti-STFK IgG1, **D** and **L** anti-STFK IgG2a, **E** and **M** anti-STFK IgG2b, **F** and **N** anti-STFK IgG2a:IgG1 ratio, **G** and **O** anti-STFK IgG2b:IgG1 ratio, **H** and **P** NT₅₀ of the STFK prototype or BA.4/5 were assessed, *n* = 6 per group. **Q** and **R** Anti-STFK and anti-RBD binding titers of immune sera from young and aged C57BL/6 mice from Week 1 to Week 10 or Week 8. The data were log-transformed and tested employing Mann–Whitney U test. **p* < 0.05, ***p* < 0.01, ****p* < 0.001

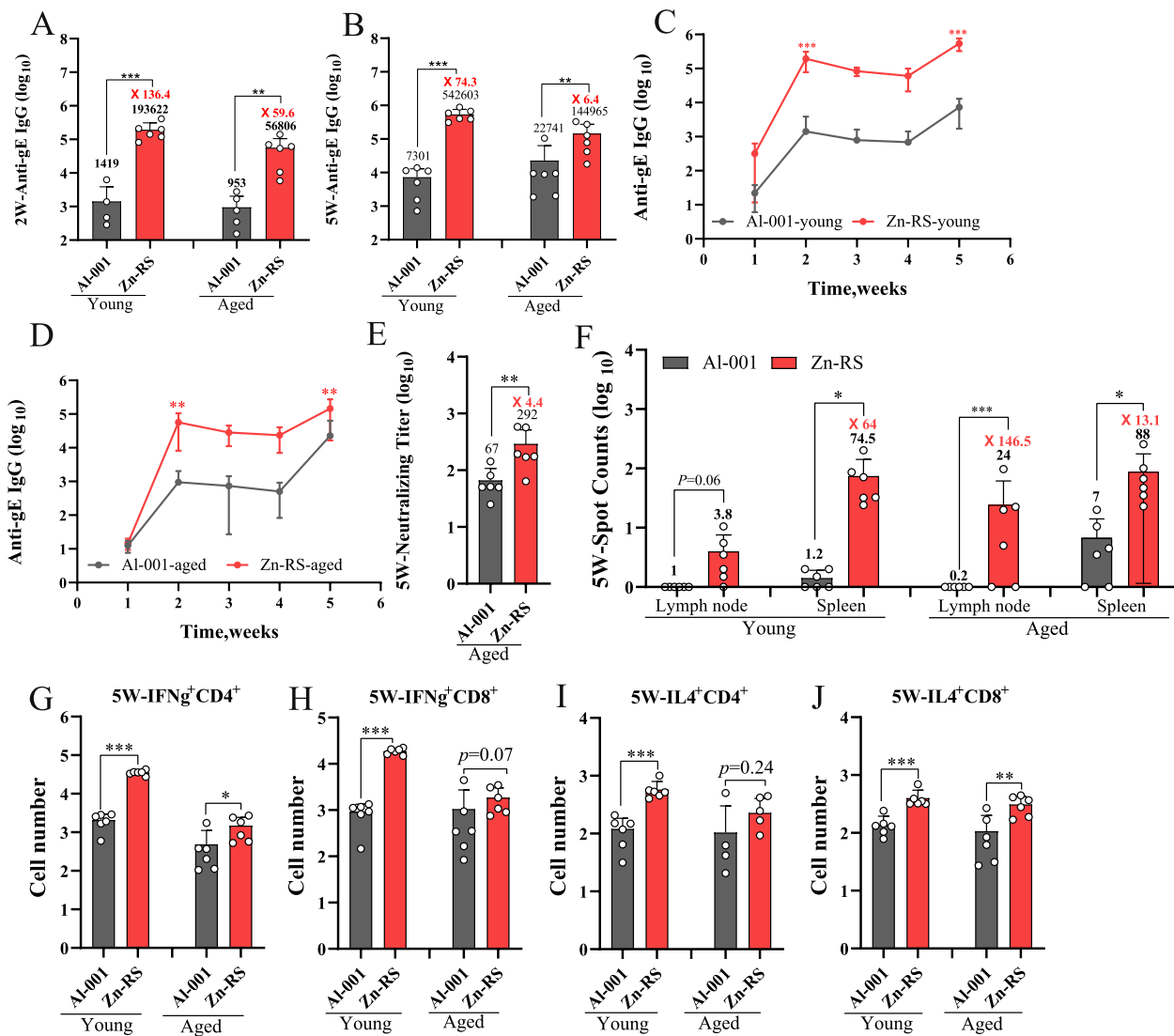


Fig. 3 Zn-RS-adjuvanted gE elicited potent immune responses in young and aged mice. Young adult, 6-week-old C57BL/6 and aged, 15-month-old C57BL/6 mice received intramuscular injections on days 0 and 28 with 5 μ g of gE protein with AI-001 or Zn-RS. Retro-orbital blood was collected weekly, and **A** binding antibody titers against gE at Week 2, **B** binding antibody titers against gE at Week 5, **C** and **D** dynamic changes of binding antibody titers against gE from week 1 to week 5 (6-week-old and 15-month-old C57BL/6). **E** Neutralizing titer of only aged individuals at Week 5. **F** Spleens and lymph nodes were collected 1 week following the final immunization and then stimulated with a gE peptide pool before being subjected to ELISpot and **G** to **J** flow cytometry, $n = 6$. **F** Quantification of IFN- γ released from cells within each well was performed via ImmunoSpot software. **G** to **J** Absolute numbers of IFN- γ ⁺CD4⁺ T helper (Th1), IL-4⁺CD4⁺ T helper (Th2), IFN- γ ⁺CD8⁺ T, and IL-4⁺CD8⁺ T cells were examined via flow cytometry. Statistical significance was determined via the Mann-Whitney U test. * $p < 0.05$, ** $p < 0.01$, *** $p < 0.001$

response and accelerated antibody affinity maturation observed in two age groups of mice immunized with the Zn-RS-adjuvanted STFK vaccine. Furthermore, compared with the AI-001 formulation, the Zn-RS formulation induced greater proliferation of memory B cells and memory T cells in aged mice (Fig. 5B), which may be related to the age-associated alterations in the immune system in the two age groups.

Increased Th1/Th2/Th9/Th17 cytokine release after Zn-RS stimulation

In the late 1980s, Mossman and Coffman categorized CD4⁺ and CD8⁺ T cells into Th1 and Th2 cells based on distinct cytokine secretion patterns. Th1 cells (featured by their secretion of IFN- γ) are essential components of cellular immunity. In contrast, Th2 cells primarily release interleukin (IL)-4, IL-5, and IL-13. Th2 lymphocytes are considered as pivotal regulators of humoral immunity

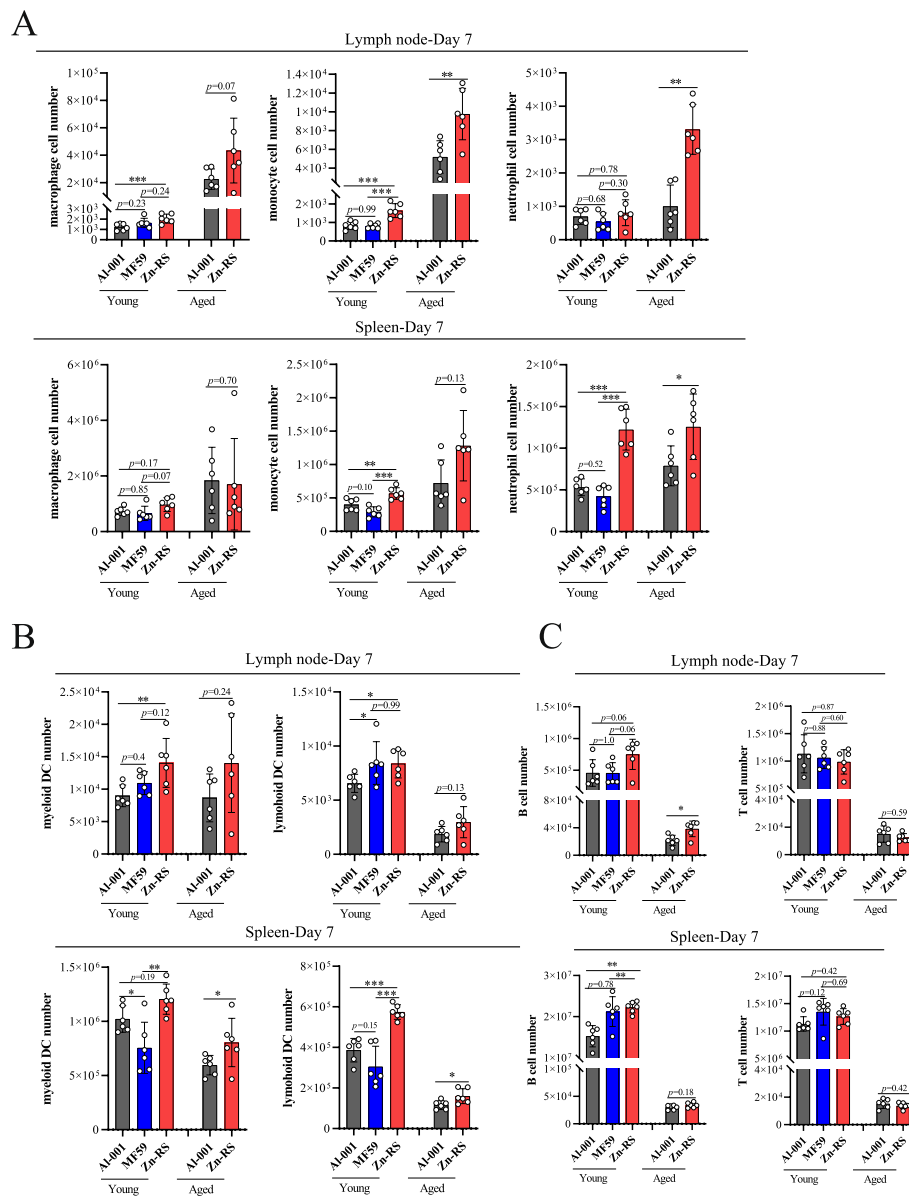


Fig. 4 The Zn-RS adjuvant formulation elicited robust APC responses. C57BL/6 mice (young adults: 6 weeks old; aged: 15 months old) received subcutaneous injections of 10 µg of the STFK1628x protein formulated with either the AI-001 or Zn-RS adjuvant following single- or double-dose immunization protocols. Spleens and draining lymph nodes were aseptically collected 7 days post-primary immunization for immune cell profiling. **A** Absolute numbers of macrophages, monocytes and neutrophils; **B** myeloid DCs and lymphocyte DCs; **C** B cells and T cells. The data are presented as the means ± SDs (n = 6/group). Statistical significance was evaluated via the Mann-Whitney U test (two-group comparison) or one-way ANOVA (multi-group comparison). *p < 0.05, **p < 0.01, ***p < 0.001

and controllers of extracellular pathogens [36]. Th9 lymphocytes are distinguished by their expression of IL-21, IL-9, and IL-10 [37]. Th17 lymphocytes constitute a distinct CD4⁺ T helper subset characterized by their secretion of cytokines such as IL-17 A/IL-17 F heterodimers. The influence of Th9 and Th17 lymphocytes on the process of carcinogenesis is predominantly dictated by the specific tissue microenvironment or cancer context [38].

Notably, the Th1 immune response caused by AI-001 or Zn-RS in aged mice was much stronger than that in young mice, whereas the Th2 immune response was largely equivalent between the two age groups (Fig. 6A), which is consistent with the imbalance of Th1/2 immune responses in the aged population mentioned in the literature. This leads to chronic inflammation in older individuals [39]. Compared with the AI-001 adjuvant, the Zn-RS

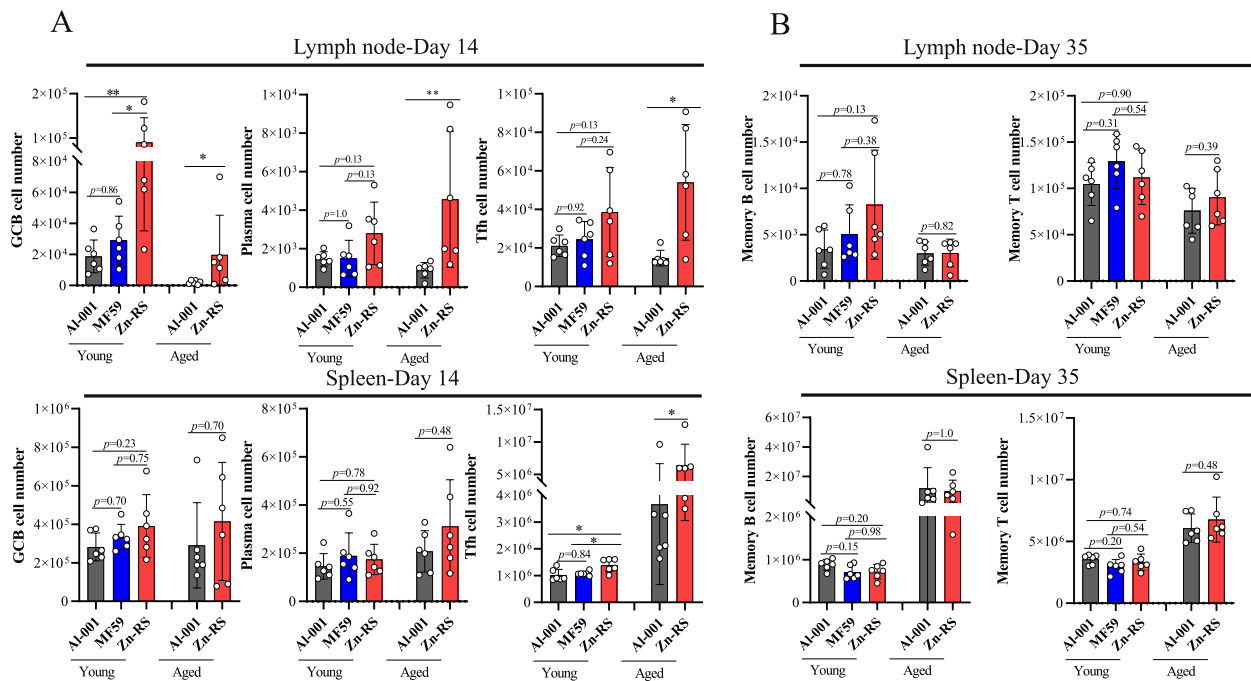


Fig. 5 The Zn-RS adjuvant formulation drove the expansion of GCB and memory B/T cells. Young adult (6-week-old) and aged (15-month-old) C57BL/6 mice were subcutaneously injected with 10 μ g of the STFK1628x protein (formulated in the AI-001 or Zn-RS adjuvant) on days 0 and 21 post-initial treatment. **A** Spleen and lymph node samples were collected 14 days post-initial injection. Absolute numbers of GCB cells, plasma cells and T_H cells. **B** Draining inguinal LNs and spleens were harvested 14 days following the second injection. Absolute numbers of memory B cells and T cells. The data are presented as the means \pm SDs ($n=6$ /group). Statistical significance was evaluated using Mann-Whitney U test (two-group comparison) or one-way ANOVA (multi-group comparison). * $p < 0.05$, ** $p < 0.01$, *** $p < 0.001$

adjuvant combined with STFK1628x [21] elicits stronger and balanced Th1 and Th2 immune responses, achieving a balanced cytokine environment (Fig. 6A, 2C-E; 2 K-M). Moreover, the Zn-RS adjuvant induced more Th9/17 cytokines than the AI-001 adjuvant did in the young and aged mice's lymph nodes and spleens (Fig. 6B). Raw flow cytometry plots for all the groups in Fig. 6, the gating strategy for the different populations (Fig. S1 A, B) and the antibody panels used is available from Supplementary data.

Discussion

The share of elderly individuals within the population worldwide is on the rise. Senior citizens are especially at risk for numerous infectious conditions, notably respiratory viruses such as SARS-CoV-2 and influenza [40]. Elderly individuals exhibit increased susceptibility to COVID-19 and demonstrate a marked predisposition toward severe illness compared with their younger counterparts. Additionally, their hospitalization and mortality rates following infection exceed those recorded in younger populations [41]. The decline in geriatric and dysregulation of immunological function, termed immunosenescence, may significantly contribute to the

heightened vulnerability of older adults to severe outcomes from SARS-CoV-2 [42]. There is an imperative requirement to develop age-tailored vaccines to optimize defensive immunity in older adults. Adjuvants are substances that enhance vaccine efficacy [43]. A good adjuvant is needed to protect aged patients from infectious diseases [44–47].

Serum neutralization potency against spike protein or receptor-binding domain contributes significantly to providing defense the progression of SARS-CoV-2 infection. The significant impact of COVID-19 infection and restricted access to efficacious therapies, particularly for elderly patients, necessitate a more systematic and rational approach to managing the disease. The development of effective cellular immunity in aged individuals is crucial for ensuring the efficacy of vaccines [48]. Herpes zoster (HZ), which differs from respiratory infections, is a viral disease that typically appears in older adults and has a pathology closely associated with a decline in cellular immunity [49]. Here, we evaluated the formulation of Zn-RS with the gE antigen or STFK in young and aged mice. And found that Zn-RS combined with the gE or STFK induced stronger humoral responses and higher neutralizing antibody titers in 6-week-old and

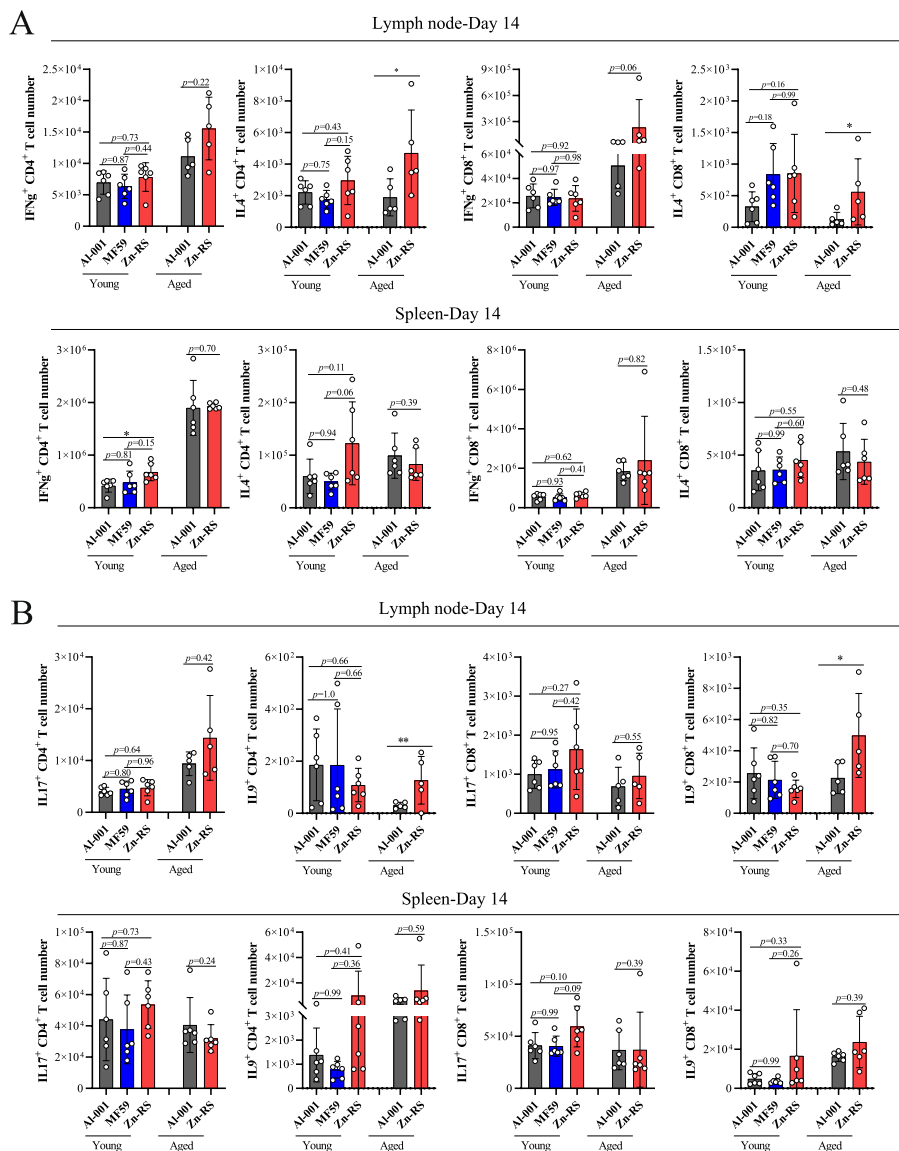


Fig. 6 The Zn-RS adjuvant formulation promoted Th1/Th2/Th9/Th17 cytokine release. Young adult (6-week-old) and aged (15-month-old) C57BL/6 mice were subcutaneously injected with 10 μ g of the STFK1628x protein (formulated in the Al-001 or Zn-RS adjuvant) following either a single or double immunization. Spleen and lymph node tissues were harvested 2 weeks post-primary injection. Flow cytometric analysis of cytokine-producing T-cell subsets: **A** IFN- γ ⁺CD4⁺ T helper (Th1) cells, IL-4⁺CD4⁺ T helper (Th2) cells, IFN- γ ⁺CD8⁺ T cells, and IL-4⁺CD8⁺ T cells. **B** IL-9⁺CD4⁺ T helper (Th9) cells, IL-17⁺CD4⁺ T helper (Th17) cells, IL-9⁺CD8⁺ T cells, and IL-17⁺CD8⁺ T cells. The data are presented as the means \pm SDs ($n = 6$ /group). Statistical significance was tested by the Mann–Whitney U test for pairwise comparisons and one-way ANOVA for multiple group comparisons. * $p < 0.05$, ** $p < 0.01$, *** $p < 0.001$

15-month-old mice. Moreover, in 15-month-old mice, compared with Al-001, Zn-RS prolonged humoral immunity. At the same time, the Zn-RS formulation elicited a Th1-type immune response bias and stronger T-cell response than the aluminum formulation did in young and aged mice.

Recently, regulatory authorization has been granted to MF59[®]-adjuvanted influenza vaccines (FluadTM), despite incomplete characterization of this

emulsion-based adjuvant’s mechanism of action. Alternatively, authorization for employing the Fluzone[®] high-dose vaccine in the United States began in 2009. Additionally, these vaccines were not intentionally designed to compensate for the particular inefficiencies in the mechanisms of aging B cells. Instead, their formulations progressed through the clinical trial phases, primarily because they enhance overall vaccine effectiveness. While these vaccines can induce elevated

protective antibody levels among older individuals, the precise mechanisms through which they provoke such robust immune responses remain incompletely elucidated. Understanding the functional mechanisms of adjuvants has been crucial to their successful use in enhancing immune responses, which can guide the strategic development of novel vaccine formulations that target diseases sharing comparable biological characteristics. Here, we combined Zn-RS with STFK1628x [21] and reported that it induced similar proliferation of immune cells in young and old animals, with greater increases in DCs, APCs, GCBs, plasma cells, T_{FH} cells, and other lymphocytes in older mice, suggesting its potential as a vaccine adjuvant for the elderly and providing a basis for the development of other adjuvants that target this population by promoting similar immune cells. Additionally, to gain deeper mechanistic insight into Zn-RS, our study will concentrate on elucidating the transcriptomic differences between immune responses elicited by Zn-RS and those induced by AI-001, aiming to clarify the mechanisms of Zn-RS and contribute to the progression of personalized vaccination strategies designed specifically for seniors.

In addition to efficacy, safety is equally critical in vaccine development, particularly for populations such as the elderly, who have diminished immunity and tolerance. This study demonstrated that Zn-RS exhibited excellent safety in KM mice. Next, we will also study the safety of Zn-RS in SD rats of different ages and in BALB/c mice. Also, neurotoxicity and long-term toxicity should be taken into consideration. For elderly patients receiving bisphosphonate therapy for osteoporosis prevention, antibodies targeting bisphosphonates deserve attention due to potential treatment interference. Then the absence of reported antibody-mediated bisphosphonate depletion in osteoporosis patients [50, 51] underscores the minimal risk of antibody development in clinical use. Moreover, vaccination protocols typically involve a significantly reduced dosing burden compared to clinical treatment. Nevertheless, future trials incorporating immunogenicity assays could help clarify this risk, particularly for patients undergoing concurrent vaccinations or immunomodulatory therapies.

In conclusion, Zn-RS combined with VZV gE or STFK induces higher binding and neutralizing antibody titers in two age groups (6 weeks old and 15 months old) than does an aluminum adjuvant. Additionally, prolonged binding enhances antibody effectiveness. Zn-RS also increases the production of DCs, APCs, GCBs, plasma cells, T_{FH} cells, and other lymphocytes in aged mice, offering valuable insights for the exploration of novel vaccine adjuvant systems for older adults.

Materials and methods

Designation of the study

This study aimed to explore the enhanced immune response of Zn-RS adjuvant in aged mice. The mechanism was then explored preliminarily. Sample size estimation was empirically optimized to accommodate result variability and meet statistical potency requirements, while also minimizing animal participation in accordance with the ethical principle of reduction. Two age groups (young adults: 6 weeks old; aged: 15 months old) C57BL/6 mice were randomly allocated into experimental cohorts ($n = 6$ per group) for measurement of antibody titers and assessment of different immune system responses. For the abnormal toxicity assay, six KM mice were randomly allocated to each group for the experimental study. The study was conducted without blinding procedures, and experimental replication numbers varied among the experiments, with details provided in the figure legends.

Animals

All the animals utilized in the study, including female C57BL/6 mice (6 weeks old) and female KM mice (5 weeks old), were provided by Shanghai SLAC Laboratory Animal Co., Ltd. Female, 15-month-old C57BL/6 mice were acquired from Xiamen University Laboratory Animal Center. All animal experiments were performed following the strict guidelines provided by the *Guide for the Care and Use of Laboratory Animals*. The mice were euthanized by cervical dislocation when the experiments were ended. For the mice used for the mechanistic study, their draining lymph nodes (dLNs) and spleens were harvested. Consideration was given to animal welfare, with efforts made to minimize potential suffering.

Preparation and characterization of the Zn-RS and AI-001 adjuvants

AI-001 represents aluminum salt adjuvant, while Zn-RS represents the adjuvant composed of Zn^{2+} , risedronate, and phosphate. The key technique employed for creating this adjuvant is termed T-mixing, which ensures the uniform mixing of its various components [20]. The AKTA purifier liquid chromatography system facilitated precise and uniform mixing at a constant flow rate of 100 mL/min. The liquid containing Zn^{2+} or Al^{3+} served as Solution A, whereas the liquid containing phosphate or a mixture of risedronate and phosphate acted as Solution B. To ensure that the final pH of the adjuvant was close to the neutral pH of humans, we adjusted the pH of Solution B to approximately 7.5 by adding NaOH reagent cautiously. After autoclaving at 121 °C for 60 min, these adjuvants were ultimately obtained, with a total metal concentration of approximately 31 mM. For Zn-RS, the concentration of

risedronate was 3.9 mM. Furthermore, MF59 was prepared according to the established protocol for MF59TM; in contrast to Zn-RS and Al-001, MF59 utilizes a distinctive oil-in-water emulsion formulation comprising 10% (v/v) squalene and 1% (w/v) each of Tween 80 and Span 85.

Prior to characterization via JEOL JEM-1200EX transmission electron microscopy, the adjuvants were diluted by a factor of 50. Zn-RS and Al-001 were diluted to equal volumes with physiological saline and then placed into a 10 mL glass vial, which was left at room temperature for 24 h. Before and after this duration, photographs were taken to document the appearance of the adjuvant. A Nano-Brook Omni analyzer (Brookhaven) was employed to measure the hydrodynamic diameter and zeta potential of the adjuvants precisely. To characterize the adjuvants further, we employed an Agilent multi-collector inductively coupled plasma optical emission spectroscopy system, which measured the total and supernatant metal contents in the adjuvants with high accuracy. The biomineralization rate was obtained using the following formula: $[1 - (\text{supernatant metal content}/\text{total metal content})] * 100\%$. The risedronate concentrations were determined through UV/Vis absorption spectroscopy (260 nm detection wavelength) with a DU800 system (Beckman Coulter). For the quantification of risedronate, calibration curves were established based on the optical density (OD₂₆₀) measured from a series of risedronate standards at the following concentrations: 0.16, 0.08, 0.06, 0.04, 0.03, 0.02, 0.015, and 0.01 mg/mL. The formula used to calculate the biomineralization rate of risedronate was analogous to that employed for calculating the metal biomineralization rates.

Prior to being combined with either Zn-RS or Al-001 at a 1:1 volume ratio, the STFK underwent saline-based dilution, resulting in 200 µg/mL. And then the mixture was stored at 4 °C overnight. Following centrifugation at 13,000 r per minute for 10 min, the supernatant was used to determine absorption by ELISA with 36H6 as the coating antibody and 85 F7-HRP as the catching antibody. Adsorption rate = $[(100 - \text{STFK concentration in the supernatant})/100] * 100\%$.

To evaluate the safety of Zn-RS, we injected KM mice (6 mice per group) intraperitoneally (0.5 mL per mouse) according to the instructions of the Chinese Pharmacopoeia, with Al-001 as the control. Body weight and survival rates were recorded daily from day 0 to day 7 following their initial injection.

Adjuvants and immunization

To assess the enhancement in antibody titers of the Zn-RS adjuvant, female C57BL/6 mice in two age groups

(young adults: 6 weeks; aged: 15 months) were systematically distributed across 4 treatment cohorts ($n = 6$ per group). Each group was administered one of four distinct formulations: 1 µg of STFK with Zn-RS or Al-001 adjuvants or 5 µg of VZV gE proteins [22] with Zn-RS or Al-001 adjuvants. At the beginning of the experiment and subsequently on day 21 or 28, each mouse in all the groups received an intramuscular injection of 150 µL. For antibody titer measurement, serum samples were collected via orbital bleeding. Before analysis, the samples were first centrifuged at 13,000 r per minute for 10 min and then stored at -20 °C. For further evaluation of immune responses, an enzyme-linked immunospot assay (ELISPOT) and flow cytometry were conducted on splenocytes and lymphocytes harvested 1 week post the boost immunization. The mice involved in the mechanistic study were administrated subcutaneously with vaccines (10 µg of STFK1628x formulated with Zn-RS or Al-001 adjuvants). Like in the antibody response assessment experiment, a single dose of 150 µL or two doses were given on days 0 and 21. Following the collection of splenocytes and lymph node tissues at three time points (days 7, 14, and 35), the resulting cellular suspensions were immediately analyzed via flow cytometry.

Enzyme-linked immunosorbent assay

Before the experiment, the STFK protein was diluted to 1 µg/mL in 1 × CB9.6, coated onto 96-well plates (100 µL per well), and then incubated at 37 °C for 2 h. The wells were subsequently blocked with 1 × ED for 2 h at 37 °C. Serum samples were consecutively diluted and transferred into 96-well plates, followed by 1-h antigen-antibody-specific interactions at 37 °C. After being washed five times, horseradish peroxidase (HRP)-labeled antibodies (goat-anti-mouse IgG, IgG1, IgG2a, or IgG2b antibodies) obtained from Abcam were added to the wells separately. After being maintained at 37 °C for an additional 0.5 h, they were then reacted with tetramethylbenzidine chromogen solution (Wantai, 100 µL/well). Ten minutes later, 2 M sulfuric acid (H₂SO₄) was added to terminate the chromogenic reaction in the case of excessive color development. Finally, the absorbance at an optical density (OD) of 450–630 was read. Each plate contained six serum samples collected before the first injection, and the cutoff value was established by adding three standard deviations to the average value obtained from the six serum samples. The endpoint titer was established as the last serial dilution maintaining an optical density measurement greater than the predetermined threshold value. For anti-gE binding titer measurement, the coating solution was 1 × PBS, the sealing solution was sealing fluid-3, and the incubation time after the addition of serum was the same as that after the addition of the goat-anti-mouse

antibody conjugated with HRP (0.5 h). The serum was diluted with SD-1, and the anti-mouse horseradish peroxidase conjugates were diluted with ED-13. For the anti-RBD binding titer measurement, the coating solution was $1 \times \text{CB } 9.6$, and the other solution was the same as that used for the anti-gE binding titer measurement.

SARS-CoV-2 pseudovirus neutralizing antibody titer measurement

On the basis of our established methodology [52], neutralization assays were performed using BHK21-hACE2 cellular models challenged with pre-generated SARS-CoV-2 pseudotyped particles (based on vesicular stomatitis virus). Briefly, the cells were initially cultured in 96-well plates, and then the serum samples (tenfold serial dilutions) were incubated with pseudoviruses at 37°C under a 5% CO_2 atmosphere for 1 h. The serum-virus complexes were subsequently transformed into pre-seeded cellular monolayers and maintained under identical culture conditions for 12–16 h. Finally, fluorescence quantification was conducted through automated high-content image acquisition with the Operetta CLS System (PerkinElmer). Serum-free virus-infected wells served as positive controls for normalization of 100% infection rates. Neutralization potency was determined via four-parameter logistic regression analysis (GraphPad Prism 8), with the 50% inhibitory dilution (ID_{50}) defined as the serum dilution required to reduce pseudovirus infection by 50% relative to positive controls.

VZV-specific neutralization assay

ARPE-19 cells were utilized in the experiment, as reported previously. The study was conducted based on previous literature and our preliminary studies [53, 54]. Prior to co-culture, cells were plated and pre-incubated in 24-well plates under standard culture conditions (37°C , 5% CO_2) for 12 h. Serum samples were subjected to heat inactivation at 56°C for 0.5 h to eliminate complement proteins. The serum samples were subsequently subjected to fivefold serial dilutions via virus stabilization buffer (pH 7.4; 25 mmol/L histidine, 150 mmol/L NaCl, and 9% w/v sucrose). Each diluted serum sample was mixed with: (a) rabbit complement (1/10 of the total volume), (b) 100 plaque-forming units of cell-free virus. The virus-serum-complement mixtures were incubated at $37^\circ\text{C}/5\% \text{CO}_2$ for 60 min before being applied to the pre-seeded ARPE-19 monolayers. Following a 60-min viral adsorption phase at 37°C , the infectious medium was carefully replenished with fresh medium, and the cultures were maintained for 72 h under standard conditions. Infection efficiency was quantified via an ELISPOT assay according to established protocols [55, 56]. Serum-free

wells containing virus and complement served as positive controls for maximal infection. Neutralization antibody titers were determined as the maximum serum dilution that demonstrated $\geq 50\%$ inhibition of viral infection in the positive control wells.

Enzyme-Linked Immunospot Assay (ELISPOT)

Spleens and lymph nodes collected from the mice were ground and filtered through cell strainers. Spleen cells were resuspended in ELISPOT assay medium and standardized to a density of 1×10^6 cells per well, and the number of lymph node cells was set at 4×10^5 cells per well. They were then plated onto ELISPOT plates pre-coated with an anti-mouse IFN- γ antibody (Dakewei Biotech). These cells were subsequently incubated with gE peptides (concentration: 5 $\mu\text{g}/\text{mL}$) at $37^\circ\text{C}/5\% \text{CO}_2$ for 20 h. Wells containing the added stimulants served as positive controls, whereas those without stimulants served as negative controls. After completing the subsequent steps referring to the manufacturer's manual, the signals were scanned and counted via a CTL-ImmunoSpot S5 Analyzer. The number of IFN- γ -releasing cells in the experimental wells was determined via the following formula: (Average spot count in positive wells—Average spot count in negative wells)/6; here, the number 6 represents the number of mice in each group.

LN and spleen immunophenotyping by flow cytometry

To comprehensively evaluate the development and activation of immunocytes, we analyzed cytokine secretion from specific cell types along with the expression of phenotypic and activation markers. We initially filtered the harvested lymph nodes and spleens through a 70- μm filter to eliminate larger tissue fragments. The filtered cells were subsequently resuspended in 2% FBS-supplemented PBS, followed by ice-cold blocking with a CD16/32 antibody for 30 min. Finally stained on ice using fluorochrome-labeled monoclonal antibodies (mAbs) corresponded with immune cells for 30 min. For intracellular cytokine staining (ICS), the cells were initially incubated with pooled spiked peptides (concentration: 1.0 $\mu\text{g}/\text{mL}$) or gE peptides (concentration: 1.25 $\mu\text{g}/\text{mL}$) and then maintained in a humidified incubator at 37°C with 5% CO_2 for 18 h. For accurate detection of cells that produce cytokines, the cells were further incubated with Golgi-Plug (BD Biosciences) for another 6 h. The cells were first washed, and surface staining was performed to identify specific markers with fluorescent markers coupled with antibodies at 4°C for half an hour. BD Cytofix/Cytoperm was then utilized for cell fixation and permeabilization. After being treated with fluorochrome-conjugated mAbs for intracellular staining, the cells underwent a

45-min period on ice. Finally, the results were analyzed via a BD LSRFORTessa X-20 flow cytometry system. All the following antibodies were used in this study: anti-MHCII (PE/Cy7, BD), anti-CD11c (PerCP/Cy5.5, BD), anti-CD11b (PE, BD), anti-CD80 (FITC, Biolegend), anti-CD86 (BV421, Biolegend), anti-Ly6c (APC/Cy7, BD), anti-Ly6g (BV605, BD), anti-B220 (PE/Cy7 and FITC, Biolegend), anti-TCR β (PerCP/Cy5.5, Biolegend), anti-CD95 (PE, BD), anti-IgD (FITC, Biolegend), anti-GL-7 (APC, Biolegend), anti-CD138 (BV421, Biolegend), Purified CXCR5 (Biolegend, Biolegend), Biotin-rat IgG2a (BD), APC streptavidin (BD), anti-mouse CD8 (APC, Biolegend), anti-mouse CD4 (FITC, Biolegend), anti-mouse PD1 (BV421, Biolegend), anti-mouse IL-4 (PE, Biolegend), anti-mouse IFN- γ (APC, Biolegend), anti-mouse IL-9 (APC, BD), anti-mouse IL-17 (PE, BD), anti-mouse PD L2 (BV421, BD), anti-mouse CD73 (AF647, Biolegend), anti-mouse CCR7 (PE, Biolegend), anti-mouse CD62L (APC, BD), and anti-mouse CD44 (BV605, BD). The LLIVE/DEAD[®] Fixable Aqua Dead Cell Stain Kit was also employed to assess cell viability. For the analysis of data from the experiment, FlowJo X 10.0.7r2 was utilized, while GraphPad Prism version 8 facilitated both statistical analysis and the creation of graphs.

Ethics statement

Animal experiments were conducted with the approval of Institutional Animal Care and Use Committee of Xiamen University (Permit Number: XMULAC20190145), ensuring compliance with ethical standards. All experimental procedures involving mice were conducted in strict adherence to the guidelines established by the Chinese Regulations on Laboratory Animals and the Requirements for Laboratory Animal Environment and Housing Facilities.

Statistical analysis

Statistical analyses were performed with SPSS software (version 20.0), and graphing was achieved with GraphPad Prism 8 software. Statistical details are provided in the figure legends. All the data are presented as the means \pm standard deviations (SDs). The definition of statistical significance was as follows: * $p < 0.05$, ** $p < 0.01$, *** $p < 0.001$.

Supplementary Information

The online version contains supplementary material available at <https://doi.org/10.1186/s12979-025-00512-0>.

Supplementary Material 1.

Acknowledgements

This work was funded by the National Key Research and Development Program of China (2024YFC2311004) and National Natural Science Foundation of China grants (82322027, 32170943, and 82341043).

Authors' contributions

Yue Liu: writing the original draft, providing resources, and reviewing and editing the manuscript. Man Yang: Data analysis, experimental performance. Meifeng Nie: experimental design. Shuyu Wu and Rong Su: resources. Dekui Qiu and Shouneng Lu: investigation. Hualong Xiong and Jinlei Zhang: methodology. Shengxiang Ge: resources, investigation. Quan Yuan: supervision, methodology. Qinjian Zhao: supervision, resources. Tianying Zhang: funding acquisition, supervision, methodology, resources. Yingbin Wang: project administration, resources. Ningshao Xia: funding acquisition, supervision, project administration, investigation. All the authors reviewed and accepted the definitive manuscript, confirming that all the contributions and revisions were accurately incorporated.

Data availability

No datasets were generated or analysed during the current study.

Declarations

Competing interests

The authors declare no competing interests.

Received: 16 February 2025 Accepted: 24 April 2025

Published online: 13 May 2025

References

- Mascola JR, Fauci AS. Novel vaccine technologies for the 21st century [J]. *Nat Rev Immunol*. 2020;20(2):87–8.
- Hou YY, Chen M, Bian Y, et al. Advanced subunit vaccine delivery technologies: From vaccine cascade obstacles to design strategies [J]. *Acta Pharm Sin B*. 2023;13(8):3321–38.
- Bell MR, Kutzler MA. An old problem with new solutions: Strategies to improve vaccine efficacy in the elderly [J]. *Adv Drug Deliver Rev*. 2022;183:114175.
- Hou YY, Chen M, Bian Y, et al. Insights into vaccines for elderly individuals: from the impacts of immunosenescence to delivery strategies [J]. *Npj Vaccines*. 2024;9(1):77.
- Moni SS, Abdelwahab S I, Jabeen A, et al. Advancements in Vaccine Adjuvants: The Journey from Alum to Nano Formulations [J]. *Vaccines-Basel*. 2023;11(11):1704.
- Zhivaki D, Kennedy S N, Park J, et al. Correction of age-associated defects in dendritic cells enables CD4+T cells to eradicate tumors [J]. *Cell*. 2024;187(15):3888–3903.e18.
- Russell R G, Fleisch H. Pyrophosphate and diphosphonates in skeletal metabolism. Physiological, clinical and therapeutic aspects [J]. *Clin Orthop Relat Res*. 1975;(108):241–63.
- Johansen A, Stone M, Rawlinson F. Bisphosphonates and the treatment of bone disease in the elderly [J]. *Drugs Aging*. 1996;8(2):113–26.
- Kunzmann V, Bauer E, Wilhelm M. Gamma/delta T-cell stimulation by pamidronate [J]. *N Engl J Med*. 1999;340(9):737–8.
- Chen YJ, Chao KS, Yang YC, et al. Zoledronic acid, an aminobisphosphonate, modulates differentiation and maturation of human dendritic cells [J]. *Immunopharmacol Immunotoxicol*. 2009;31(3):499–508.
- Nie MF, Wu SY, Chen YY, et al. Micronanoparticled risedronate exhibits potent vaccine adjuvant effects [J]. *J Control Release*. 2024;365:369–83.
- Tamura Y. The Role of Zinc Homeostasis in the Prevention of Diabetes Mellitus and Cardiovascular Diseases [J]. *J Atheroscler Thromb*. 2021;28(11):1109–22.
- Poli V, Pui-Yan Ma V, Di Gioia M, et al. Zinc-dependent histone deacetylases drive neutrophil extracellular trap formation and potentiate local and systemic inflammation [J]. *iScience*. 2021;24(11):103256.

14. Nitz M, Smith D, Wysocki B, et al. Modeling of an immune response: Queuing network analysis of the impact of zinc and cadmium on macrophage activation [J]. *Biotechnol Bioeng.* 2021;118(1):412–22.
15. Wessels I, Fischer HJ, Rink L. Update on the multi-layered levels of zinc-mediated immune regulation [J]. *Semin Cell Dev Biol.* 2021;115:62–9.
16. Ollig J, Kloubert V, Taylor KM, et al. B cell activation and proliferation increase intracellular zinc levels [J]. *J Nutr Biochem.* 2019;64:72–9.
17. Wessels I, Rolles B, Slusarenko AJ, et al. Zinc deficiency as a possible risk factor for increased susceptibility and severe progression of Corona Virus Disease 19 [J]. *Brit J Nutr.* 2022;127(2):214–32.
18. Gombart AF, Pierre A, Maggini S. A Review of Micronutrients and the Immune System-Working in Harmony to Reduce the Risk of Infection [J]. *Nutrients.* 2020;12(1):236.
19. Wang X, Yin XC, Zhang BY, et al. A prophylactic effect of aluminium-based adjuvants against respiratory viruses via priming local innate immunity [J]. *Emerg Microbes Infect.* 2022;11(1):914–25.
20. Wu YT, Huang XF, Yuan LZ, et al. A recombinant spike protein subunit vaccine confers protective immunity against SARS-CoV-2 infection and transmission in hamsters [J]. *Sci Transl Med.* 2021;13(606):eabg1143.
21. Wu Y, Wang S, Zhang Y, et al. Lineage-mosaic and mutation-patched spike proteins for broad-spectrum COVID-19 vaccine [J]. *Cell Host Microbe.* 2022;30(12):1732–44.e7.
22. Xue WH, Li TT, Zhang SB, et al. Baculovirus Display of Varicella-Zoster Virus Glycoprotein E Induces Robust Humoral and Cellular Immune Responses in Mice [J]. *Viruses-Basel.* 2022;14(8):1785.
23. Shah RR, O'Hagan DT, Amiji MM, et al. The impact of size on particulate vaccine adjuvants [J]. *Nanomedicine-Uk.* 2014;9(17):2671–81.
24. Garcia-Beltran WF, Lam EC, St Denis K, et al. Multiple SARS-CoV-2 variants escape neutralization by vaccine-induced humoral immunity [J]. *Cell.* 2021;184(9):2523.
25. Kuzmina A, Khalaila Y, Voloshin O, et al. SARS-CoV-2 spike variants exhibit differential infectivity and neutralization resistance to convalescent or post-vaccination sera [J]. *Cell Host Microbe.* 2021;29(4):522–8 e2.
26. Sun L, Wang X, Saredy J, et al. Innate-adaptive immunity interplay and redox regulation in immune response [J]. *Redox Biol.* 2020;37:101759.
27. Pollard AJ, Bijker EM. A guide to vaccinology: from basic principles to new developments [J]. *Nat Rev Immunol.* 2021;21(2):83–100.
28. Grant SM, Lou M, Yao L, et al. The lymph node at a glance - how spatial organization optimizes the immune response [J]. *J Cell Sci.* 2020;133(5):jcs241828.
29. Acton SE, Sousa CRE. Dendritic cells in remodeling of lymph nodes during immune responses [J]. *Immunol Rev.* 2016;271(1):221–9.
30. Li APY, Cohen CA, Leung NHL, et al. Immunogenicity of standard, high-dose, MF59-adjuvanted, and recombinant-HA seasonal influenza vaccination in older adults [J]. *NPJ Vaccines.* 2021;6(1):25.
31. Khurana S, Verma N, Yewdell J W, et al. MF59 adjuvant enhances diversity and affinity of antibody-mediated immune response to pandemic influenza vaccines [J]. *Sci Transl Med.* 2011;3(85):85ra48.
32. Vinuesa CG, Linterman MA, Yu D, et al. Follicular Helper T Cells [J]. *Annu Rev Immunol.* 2016;34:335–68.
33. Oracki SA, Walker JA, Hibbs ML, et al. Plasma cell development and survival [J]. *Immunol Rev.* 2010;237(1):140–59.
34. Lee SK, Rigby RJ, Zotos D, et al. B cell priming for extrafollicular antibody responses requires Bcl-6 expression by T cells [J]. *J Exp Med.* 2011;208(7):1377–88.
35. Olatunde AC, Hale JS, Lamb TJ. Cytokine-skewed Tfh cells: functional consequences for B cell help [J]. *Trends Immunol.* 2021;42(6):536–50.
36. Liu Y, Lam D M K, Luan M, et al. Recent development of oral vaccines (Review) [J]. *Exp Ther Med.* 2024;27(5):223.
37. Cannon A, Pajulas A, Kaplan MH, et al. The Dichotomy of Interleukin-9 Function in the Tumor Microenvironment [J]. *J Interf Cytok Res.* 2023;43(6):229–45.
38. Muranski P, Boni A, Antony PA, et al. Tumor-specific Th17-polarized cells eradicate large established melanoma [J]. *Blood.* 2008;112(2):362–73.
39. Crooke SN, Ovsyannikova IG, Poland GA, et al. Immunosenescence: A systems-level overview of immune cell biology and strategies for improving vaccine responses [J]. *Exp Gerontol.* 2019;124:110632.
40. Nanishi E, Angelidou A, Rotman C, et al. Precision Vaccine Adjuvants for Older Adults: A Scoping Review [J]. *Clin Infect Dis.* 2022;75(Suppl 1):S72–80.
41. Xu K, Wang Z H, Qin M R, et al. A systematic review and meta-analysis of the effectiveness and safety of COVID-19 vaccination in older adults [J]. *Front Immunol.* 2023;14:1113156.
42. Liu Z Q, Liang Q M, Ren Y Q, et al. Immunosenescence: molecular mechanisms and diseases [J]. *Signal Transduct Tar.* 2023;8(1):200.
43. Pulendran B, Arunachalam PS, O'Hagan DT. Emerging concepts in the science of vaccine adjuvants [J]. *Nat Rev Drug Discov.* 2021;20(6):454–75.
44. Nanishi E, Borriello F, O'Meara T R, et al. An aluminum hydroxide:CpG adjuvant enhances protection elicited by a SARS-CoV-2 receptor binding domain vaccine in aged mice [J]. *Sci Transl Med.* 2022;14(629):eabj5305.
45. Jangra S, Landers J J, Laghlali G, et al. Multicomponent intranasal adjuvant for mucosal and durable systemic SARS-CoV-2 immunity in young and aged mice [J]. *Npj Vaccines.* 2023;8(1):96.
46. Bai S, Kang YL, Chen WX, et al. Comparison of Immunogenicity of Alum and MF59-Like Adjuvant Inactivated SARS-CoV-2 Vaccines Against SARS-CoV-2 Variants in Elderly Mice [J]. *Viral Immunol.* 2023;36(8):526–33.
47. Gary E N, Tursi N J, Warner B M, et al. Adenosine deaminase augments SARS-CoV-2 specific cellular and humoral responses in aged mouse models of immunization and challenge [J]. *Front Immunol.* 2023;14:1138609.
48. Biswas A, Mandal RS, Chakraborty S, et al. Tapping the immunological imprints to design chimeric SARS-CoV-2 vaccine for elderly population [J]. *Int Rev Immunol.* 2022;41(4):448–63.
49. Crooke SN, Ovsyannikova IG, Poland GA, et al. Immunosenescence and human vaccine immune responses [J]. *Immun Ageing.* 2019;16:25.
50. Ebetino F H, Sun S T, Cheria P, et al. Bisphosphonates: The role of chemistry in understanding their biological actions and structure-activity relationships, and new directions for their therapeutic use [J]. *Bone.* 2022;156:116289.
51. Papapetrou PD. Bisphosphonate-associated adverse events [J]. *Horm-Int J Endocrinol.* 2009;8(2):96–110.
52. Xiong HL, Wu YT, Cao JL, et al. Robust neutralization assay based on SARS-CoV-2 S-protein-bearing vesicular stomatitis virus (VSV) pseudovirus and ACE2-overexpressing BHK21 cells [J]. *Emerg Microbes Infect.* 2020;9(1):2105–13.
53. Tsetsarkin KA, Maximova OA, Liu G, et al. Routes of Zika virus dissemination in the testis and epididymis of immunodeficient mice [J]. *Nat Commun.* 2018;9(1):5350.
54. Xue W, Li T, Zhang S, et al. Baculovirus Display of Varicella-Zoster Virus Glycoprotein E Induces Robust Humoral and Cellular Immune Responses in Mice [J]. *Viruses.* 2022;14(8):1785.
55. Chen TT, Sun J, Zhang SB, et al. Truncated glycoprotein E of varicella-zoster virus is an ideal immunogen for -based vaccine design [J]. *Sci China Life Sci.* 2023;66(4):743–53.
56. Chen LH, Liu J, Wang W, et al. Development of a varicella-zoster virus neutralization assay using a glycoprotein K antibody enzyme-linked immunosorbent spot assay [J]. *J Virol Methods.* 2014;200:10–4.

Publisher's Note

Springer Nature remains neutral with regard to jurisdictional claims in published maps and institutional affiliations.